

Mechanism and Kinetics of the Ethylene Removal in Flue Gas by Ozone Injection

ZHENGCHENG WEN*[†], ZHIHUA WANG[†], JIANGRONG XU, JUNHU ZHOU[†] and KEFA CEN[†]

School of Science, Hangzhou Dianzi University, Hangzhou 310018, P.R. China

Fax: (86)(571)87951616; Tel: (86)(571)87953162; E-mail: wenzc@hdu.edu.cn; giani@zju.edu.cn

The ozone injection is one of the promising technologies to remove multi-pollutants such as NO_x, SO₂, Hg and VOCs in flue gas simultaneously. However, little attention has been paid to the mechanism and kinetic of the volatile organic compounds (VOCs) removal during ozone injection. As well known, quantum chemical calculation is an effective means for mechanism and kinetic studies. Therefore, the mechanism and kinetic of the volatile organic compounds removal in flue gas by ozone injection were investigated in detail by employing quantum chemical calculation. Based on geometry optimizations made by B3LYP/6-31G (d) method, the microcosmic reaction processes were analyzed and depicted in detail and the reaction activation energies were calculated by QCISD(T)/6-311g(d,p) method. Moreover, the kinetic parameters of the reactions were calculated by the classical transition state theory. Results showed that, the activation energies of the C₂H₄ + O₃ and C₂H₄ + NO₃ reactions were 6.58 and 6.66 kcal/mol, respectively and the Arrhenius expressions of these two reactions were $k = 9.45 \times 10^{11} \exp(-30834/RT)$ and $k = 9.47 \times 10^{12} \exp(-31111/RT)$ (cm³ mol⁻¹ s⁻¹), respectively. The calculated activation energies and kinetic parameters were in good agreement with the experimental results, which indicated the mechanism and kinetic study by employing quantum chemical calculation was reasonable and reliable.

Key Words: Ozone, Volatile organic compounds, Ethylene, Kinetic, Removal, Quantum chemical calculation.

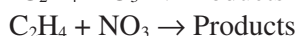
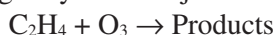
INTRODUCTION

Emissions such as NO_x, SO₂, mercury and volatile organic compounds (VOCs) during coal combustion is harmful to our atmosphere. So far, individual control of pollutions is not only larger investment, but also additional application expenses needed. The simultaneous removal of multi-pollutants in flue gas has become a recent concern on the part of the electric utility industry. A lot of high efficiency and low cost simultaneous removal of multi-pollutants technologies have been carried out, including non-thermal plasma, electric beam irradiation and adsorption process, *etc.*¹⁻³.

[†]State Key Laboratory of Clean Energy Utilization (Zhejiang University), Hangzhou 310027, P.R. China.

The technology of ozone injection is one of the most promising multi-pollutants simultaneous removal technologies for high efficiency, high energy-efficient and low cost⁴⁻⁸. The ozone injection technology achieved NO_x, SO₂, Hg and VOCs removal simultaneously by using ozone to convert NO, Hg⁰ into NO₂ and Hg²⁺, which can be captured in wet chemical scrubbers. Many efforts has been made to investigate the mechanism and kinetic of the ozone injection technology. Cannon Technology Inc. in collaboration with BOC Gases investigated the removal of NO_x in flue gas by ozone injection firstly⁴. The simultaneous removal of NO_x and SO₂ by ozone injection was investigated in a bench scale test facility by Mok *et al.*⁶. The mechanism and kinetics of the simultaneous removal of NO_x, SO₂ and Hg in flue gas by ozone injection was investigated in previous works^{7,8}. However, little attention has been paid to the mechanism and kinetics of the removal of VOCs in flue gas by ozone injection. In order to further improve the technology of ozone injection, the investigation of the mechanism and kinetic of the VOCs removal in flue gas by ozone injection is essential.

Alkenes, which are important volatile organic compounds in flue gas, were selected as typical VOCs in this paper. For the simplicity of calculation, ethylene, the simplest alkene, was selected as the typical alkene in the present study. The mechanism and kinetics of the ethylene removal in flue gas by ozone injection was investigated by employing Quantum chemical calculation in this paper. Previous investigations indicated that, strong oxidizing radicals such as O₃ and NO₃ are generated in flue gas by ozone injection^{6,7} and both O₃ and NO₃ radicals have strong ability to degrade alkenes such as ethylene⁹⁻¹¹. Therefore, the following reactions were calculated and analyzed in detail to investigate the mechanism and kinetic of the ethylene removal in flue gas by ozone injection.



CALCULATION DETAILS

Gaussian 2003 package¹² was used in the present Quantum Chemical calculations. All the geometry optimizations of stationary points along the reactions were made by the quantum chemistry B3LYP method at 6-31g(d) basis function level^{13,14}. The optimized stationary points were characterized as intermediates or transition states by diagonalizing the Hessian matrix and analyzing the vibrational normal modes. In this way, the stationary points can be classified as intermediates if no imaginary frequencies are shown or as transition states if only one imaginary frequency is obtained. Furthermore, the particular nature of the transition states was determined by the calculation of intrinsic reaction coordinate (IRC)¹⁵ and the vibrational analysis of imaginary frequency.

Based on geometry optimizations made by B3LYP/6-31G(d) method, the potential energies of stationary points of reactions were calculated by QCISD(T)/6-311g(d,p) method^{16,17}. After corrected with Zero-point energies (ZPE), the activation energies

(ΔE) of reactions were obtained. In addition, the enthalpies variation along reaction processes were also calculated and analyzed by B3LYP/6-31G(d) method, according to the equation below¹⁸:

$$\Delta H(T) = \Delta E^\circ + \Delta H_{\text{corr}}(T)$$

here, T is the temperature, ΔE° is the energy difference between products and reactants at 0 K, ΔH_{corr} is the difference of thermal energy correction to enthalpy between products and reactants.

In order to obtain more reliable values, the raw calculated values of ZPE and ΔH_{corr} were scaled by 0.9613 to account for their average overestimation when B3LYP/6-31g(d) method was employed¹⁹.

According to the calculation and analyses on the reaction processes and reaction mechanism, the reaction rate constant was calculated by transition state theory (TST). The rate constants were defined by the following rate equation of the classic transition state theory.

$$k(T) = \lambda(k_B T/h)(Q^\ddagger/Q_A Q_B) \exp(-E_a/RT)$$

$$\lambda = 1 + (h\nu^\ddagger/k_B T)^2/24$$

here, λ is the correct factor for the quantum effect, k_B is Boltzman constant, h is Planck constant, Q^\ddagger is the partial function of transition state, ν^\ddagger is the imaginary vibrational frequency of transition state, Q_A and Q_B are the partial functions of reactants, respectively, E_a is the activation energy, Q is the multiplier of transitional (Q_t), rotational (Q_r) and vibrational (Q_v) partial function, which has the relationship as $Q = Q_t Q_r Q_v$.

RESULTS AND DISCUSSION

Reaction processes: The mechanism of the $C_2H_4 + O_3$ and $C_2H_4 + NO_3$ reactions were investigated in detail by employing Quantum Chemical calculation. The geometry optimizations of stationary points such as reactants, products, intermediates (M) and transition states (TS) along reaction processes were made by B3LYP/6-31g(d) method. Based on the analysis of each stationary point, the microcosmic reaction processes were depicted in Fig. 1 and 2.

As shown in Fig. 1, the reaction process of $C_2H_4 + O_3$ can be divided as four steps, which were discussed as follows.

Formation of C_2H_4 -POZ: The primary ozonide of ethylene (C_2H_4 -POZ) is formed by the cycloaddition of ozone to ethylene. It is the first step of the reaction. During this step, a transition state (TS1) is found to connect the reactant and the C_2H_4 -POZ. As shown in Fig. 1, the distance between C atom of C_2H_4 and the terminal O atom of O_3 reduces gradually ($\infty \text{ \AA} \rightarrow 2.082 \text{ \AA} \rightarrow 1.425 \text{ \AA}$, ∞ denotes the distance exceeding the range of bond formation. The distance between the terminal O atom and the centre O atom of O_3 increases gradually ($1.264 \text{ \AA} \rightarrow 1.313 \text{ \AA} \rightarrow 1.447 \text{ \AA}$); the distance between two C atoms of C_2H_4 increases gradually ($1.329 \text{ \AA} \rightarrow 1.390 \text{ \AA} \rightarrow 1.558 \text{ \AA}$). All the changes of geometric configurations indicated the forming of C_2H_4 -POZ. Moreover, it should be noticed that there is a transition state (TS2) formed for

the self-isomerization of the symmetry-allowed C_2H_4 -POZ. As shown in Fig. 1, the changes of dihedral angle of O-C-C-O ($0^\circ \rightarrow -46.4^\circ \rightarrow 0^\circ$) can depict the self-isomerization of the C_2H_4 -POZ clearly.

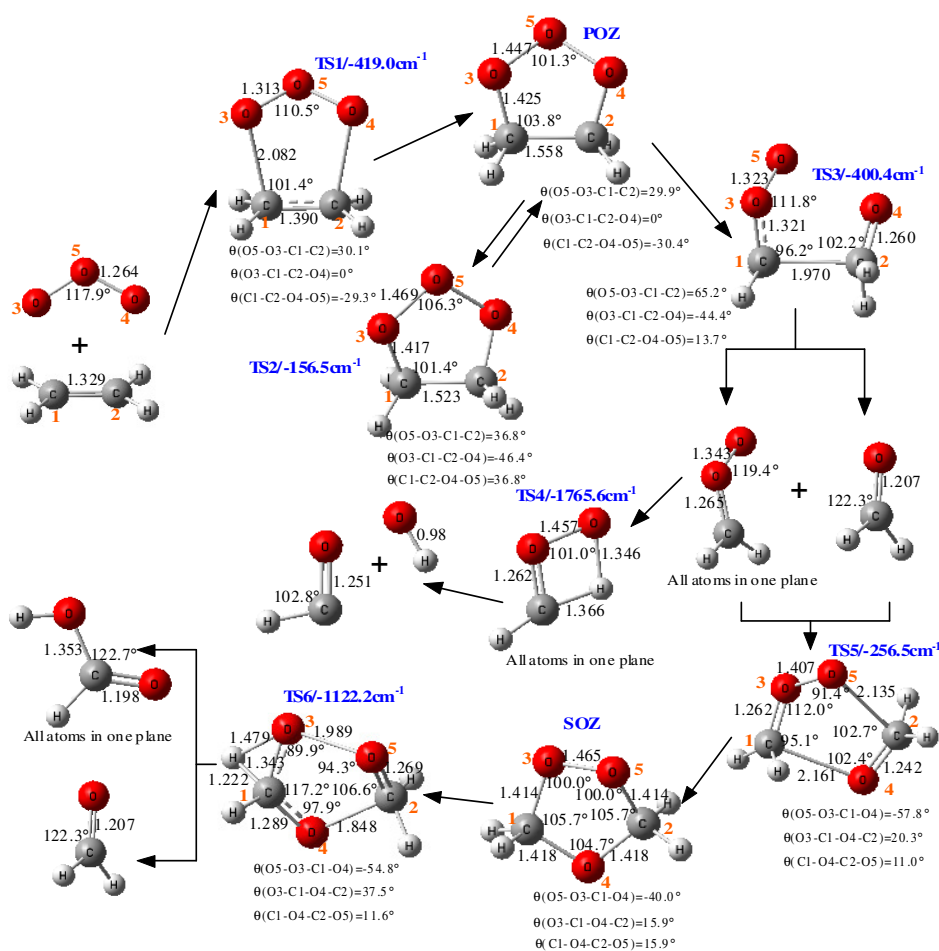


Fig. 1. Optimized geometries of the stationary points along the $C_2H_4 + O_3$ reaction process. Angles are given in degrees and bond distances are given in angstroms

Cleavage of C_2H_4 -POZ: This is an important step of the reaction, because the cleavage of C_2H_4 -POZ means the breaking of the C=C bond, which stands for the degradation of ethylene. The Criegee intermediates (HCHOO and HCHO) are formed *via* the transition state (TS3). During this step, the distance between two C atoms increases gradually ($1.558\text{\AA} \rightarrow 1.970\text{\AA} \rightarrow \infty\text{\AA}$). This change indicates the breaking of C=C bond and the cleavage of C_2H_4 -POZ. For the Criegee intermediate HCHOO, there are two competitive reaction routes. One route is the decomposition of the Criegee intermediate HCHOO. As shown in Fig. 1, the products (HCO and

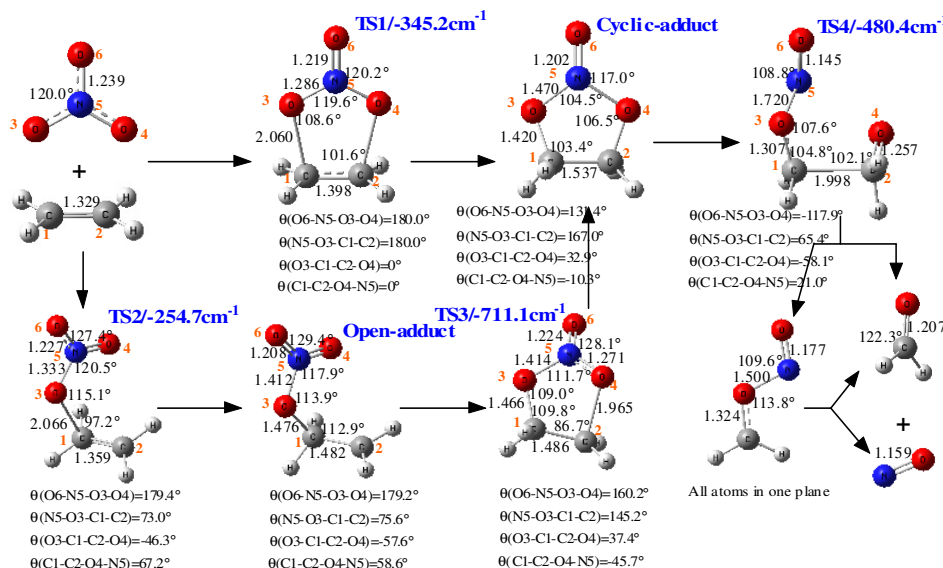


Fig. 2. Optimized geometries of the stationary points along the $C_2H_4 + NO_3$ reaction process. Angles are given in degrees and bond distances are given in angstroms

OH) are formed *via* the transition state (TS6). During the decomposition, the distance between the terminal O atom and H atom reduces gradually ($2.462\text{\AA} \rightarrow 1.345\text{\AA} \rightarrow 0.980\text{\AA}$) and the distance between the H atom and C atom increases gradually ($1.086\text{\AA} \rightarrow 1.366\text{\AA} \rightarrow \infty\text{\AA}$). The changes of bond distance indicated the formation of O-H bond and the breaking of H-C bond. The other route is the formation of the ethylene second ozonide ($C_2H_4\text{-SOZ}$) *via* the reaction between HCHO and HCHO.

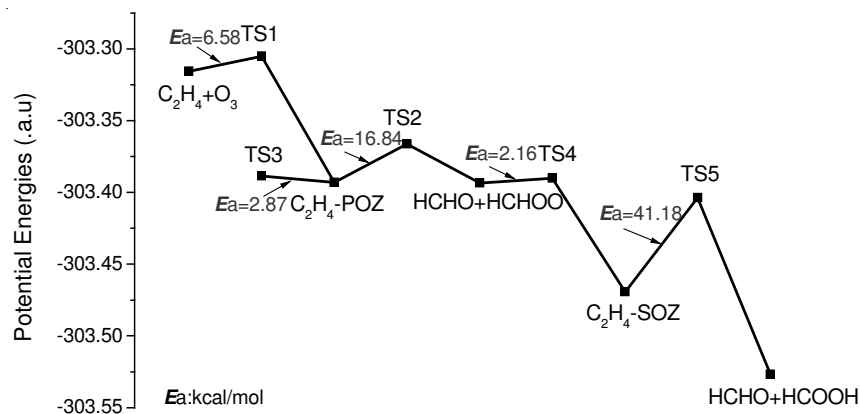
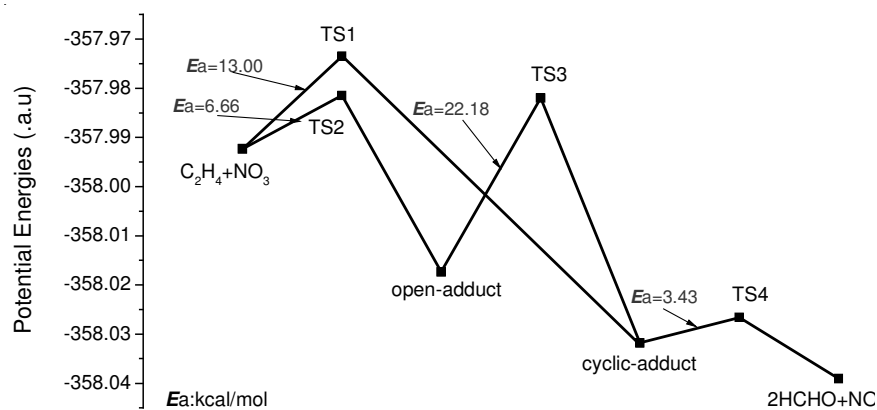
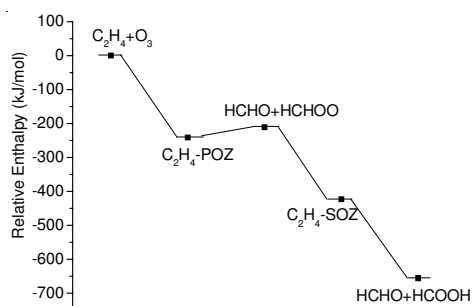
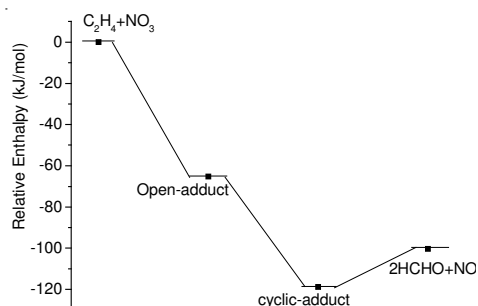
Formation of $C_2H_4\text{-SOZ}$: This step is very similar to the formation of the $C_2H_4\text{-POZ}$. The $C_2H_4\text{-SOZ}$ is formed *via* the transition state (TS4). During the formation, the distance between O atom of HCHO and C atom of HCHO reduces gradually ($\infty\text{\AA} \rightarrow 2.161\text{\AA} \rightarrow 1.418\text{\AA}$) and the distance between the terminal O atom of HCHO and C atom of HCHO reduces gradually ($\infty\text{\AA} \rightarrow 2.135\text{\AA} \rightarrow 1.414\text{\AA}$). The changes of bond distance indicated the forming of these two O-C bonds and meant the formation of the $C_2H_4\text{-SOZ}$.

Cleavage of $C_2H_4\text{-SOZ}$: This step is quite similar to the cleavage of $C_2H_4\text{-POZ}$. The products (HCHO and HCOOH) are formed *via* the transition state (TS5). As shown in Fig. 1, both the distance between two O atoms and between atom O and atom C increase gradually (O-O: $1.465\text{\AA} \rightarrow 1.989\text{\AA} \rightarrow \infty\text{\AA}$; O-C: $1.418\text{\AA} \rightarrow 1.848\text{\AA} \rightarrow \infty\text{\AA}$), which indicates the cleavage of $C_2H_4\text{-SOZ}$. Simultaneously, the distance between atom O and atom H reduces gradually ($2.022\text{\AA} \rightarrow 1.479\text{\AA} \rightarrow 0.977\text{\AA}$) and the distance between H atom and C atom increases gradually ($1.094\text{\AA} \rightarrow 1.222\text{\AA} \rightarrow 1.877\text{\AA}$). This indicates the migration of atom H and the formation of HCOOH.

As shown in Fig. 2, the reaction process of $C_2H_4+NO_3$ is quite different from the reaction process of $C_2H_4 + O_3$. Two different adducts, the open adduct and the cyclic adduct, are obtained in the addition of NO_3 to ethylene. The open adduct is formed *via* the addition of the NO_3 radical to one of the C atoms of the C=C bond, while the cyclic adduct is formed *via* the addition of the NO_3 radical to both of the two C atoms of the C=C bond. As shown in Fig. 2, the NO_3 group and the C_2H_4 group are almost vertical in the open adduct and almost horizontal in the cyclic adduct. The transition states TS1 and TS2 are obtained to connect the reactant to the cyclic adduct and the open adduct, respectively. Furthermore, the cyclic adduct and the open adduct can be transformed *via* the transition state TS3. Finally, ethylene was degraded *via* the cleavage of the cyclic adduct and the NO and formaldehyde were formed as the products *via* the transition state TS4. As shown in Fig. 2, the changes of geometric configurations about the reactants, intermediates, transition states and products can describe the reaction process of $C_2H_4 + NO_3$ clearly. Furthermore, vibration frequency analyses and IRC calculation were made to confirm the reaction processes of $C_2H_4 + O_3$ and $C_2H_4 + NO_3$. The results of vibration frequency analyses show that the intermediates don't have any imaginary vibration frequency, while every transition state have only one imaginary vibration frequency. This indicated that intermediates are the stable points of potential surface and transition states really exist. Moreover, the results of IRC calculation showed that all the transition states connected reactants to intermediates or connected intermediates to products.

Activation energies of reactions: Based on geometry optimizations made by B3LYP/6-31G (d) method above, all potential energies of stationary points along the reaction processes of $C_2H_4 + O_3$ and $C_2H_4 + NO_3$ were calculated by QCISD(T)/6-311g(d,p) method. After corrected with ZPE, the potential energies variation along the reaction processes of $C_2H_4 + O_3$ and $C_2H_4 + NO_3$ was illustrated in Figs. 3 and 4. According to the classical transition state theory (TST), the activation energy was the energy difference between unstable transition state and stable reactant or intermediate. And thus, the activation energies of all the steps of the reaction processes of $C_2H_4 + O_3$ and $C_2H_4 + NO_3$ can be obtained, which were also illustrated in Figs. 3 and 4. In addition, the enthalpies variation along reaction processes were also calculated by B3LYP/6-31G(d) method and illustrated in Figs. 5 and 6.

For the reaction of $C_2H_4 + O_3$, the formation of C_2H_4 -POZ is exothermic by 241.4 kJ/mol at 298 K (Fig. 5), which is in good agreement with the experimental results and other theoretical estimates (180-240 kJ/mol)²⁰⁻²³. Due to the exothermicity of the formation of C_2H_4 -POZ, it can be concluded that C_2H_4 -POZ is a quite stable intermediate. The formation of POZ turns out to be the rate-determining step for the whole reaction of $C_2H_4 + O_3$. As can be seen in Fig. 3, the activation energy of the formation of C_2H_4 -POZ is 6.58 kcal/mol in the present calculation. Therefore, the activation energy of the $C_2H_4 + O_3$ reaction can be fixed on 6.58 kcal/mol in the present calculation, which is comparable with the experimental results (5.4 kcal/mol)²⁴ and other theoretical calculations (5-6 kcal/mol)²¹⁻²³.

Fig. 3. Potential energies of stationary points along the reaction process of $C_2H_4 + O_3$ Fig. 4. Potential energies of stationary points along the reaction process of $C_2H_4 + NO_3$ Fig. 5. Enthalpies variation along the $C_2H_4 + O_3$ reaction process at 298 K by B3LYP/6-31G(d) methodFig. 6. Enthalpies variation along the $C_2H_4 + NO_3$ reaction process at 298 K by B3LYP/6-31G(d) method

For the reaction of $C_2H_4 + NO_3$, the formation of the open-adduct and cyclic-adduct are exothermic by 65.3 kJ/mol and 118.8 kJ/mol at 298 K, respectively, which can be seen in Fig. 6. Thus, it can be concluded that both the open-adduct and cyclic-adduct are quite stable because of the exothermicity of their formation. As shown in Fig. 4, the activation energies for forming the open-adduct and cyclic-adduct are 6.66 and 13.00 kcal/mol, respectively. Since the reaction always process along the path with lower activation energy, the formation of open-adduct can be considered as the rate-determining step for the whole reaction of $C_2H_4 + NO_3$. Therefore, the activation energy of the $C_2H_4 + NO_3$ reaction can be fixed on 6.58 kcal/mol in the present calculation, which is very close to the recommended experimental result (6.17 kcal/mol)²⁴.

Kinetic study: On the basis of the above calculation and analyses on the reaction processes, the rate constants of the $C_2H_4 + O_3$ and $C_2H_4 + NO_3$ reactions were calculated by the classical transition state theory (TST) and the results were illustrated in Fig. 7. Moreover, the Arrhenius expressions and the reaction rates at 298 K were also obtained and compared with the experimental results, which were shown in Table-1.

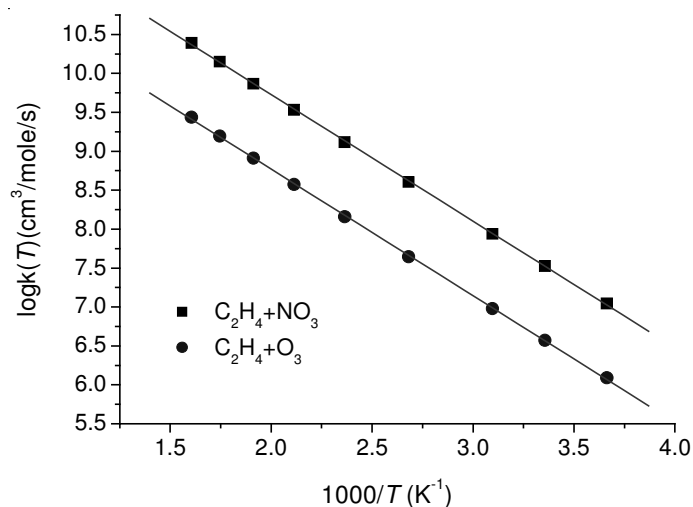


Fig. 7. Rate constant k calculated from transition state theory

TABLE-1
KINETIC PARAMETERS OF THE $C_2H_4 + O_3$ AND
 $C_2H_4 + NO_3$ REACTIONS ($k = \text{cm}^3 \text{mol}^{-1} \text{s}^{-1}$)

Reaction	$C_2H_4 + O_3 \rightarrow \text{Products}$	$C_2H_4 + NO_3 \rightarrow \text{Products}$
Arrhenius expression (TST)	$9.45 \times 10^{11} \exp(-30834/RT)$	$9.47 \times 10^{12} \exp(-31111/RT)$
Arrhenius expression (Exp.) ²⁴	$1.21 \times 10^9 \exp(-19205/RT)$	$1.99 \times 10^{12} \exp(-23932/RT)$
k^{298} (TST)	3.72×10^6	8.67×10^7
k^{298} (Exp.) ²⁴	5.51×10^5	1.35×10^8

For the reaction of $C_2H_4 + O_3$, the calculated reaction rate constant is a little larger than the experimental result (Table-1). Considering that the result obtained by theoretical calculation is the upper limit in general, the rough agreement between the calculated results and the experimental results is tolerable. For the reaction of $C_2H_4 + NO_3$, the calculated reaction rate constant is in good agreement with the experimental result (Table-1). This indicated that the mechanism and kinetic study by employing quantum chemical calculation in this paper is reasonable and reliable.

By comparing, it can be found that the calculated rate constant of the $C_2H_4 + NO_3$ reaction is more than that of the $C_2H_4 + O_3$ reaction. This finding is in good agreement with the experimental result and was also conformed in theory by Christian *et al.*²⁵. Because the activation energies of these two reactions are quite similar, the difference of the rate constants should be caused by the different preexponential factors. As can be seen in Table-1, the calculated preexponential factor A of the $C_2H_4 + NO_3$ reaction is nearly 1 order larger than that of the $C_2H_4 + O_3$ reactions. Since the rate constant of the $C_2H_4 + NO_3$ reaction is much larger than that of the $C_2H_4 + O_3$ reaction, it can be concluded that the NO_3 radical have much stronger ability to degrade ethylene than the O_3 radical.

Conclusion

The mechanism and kinetics of the ethylene removal in flue gas by ozone injection was investigated in detail by employing Quantum chemical calculation in this paper. Based on geometry optimizations made using the B3LYP/6-31G (d) method, the reaction activation energies were calculated using the QCISD(T)/6-311g(d,p) method and the kinetic parameters were calculated by the classical transition state theory. The results showed that the activation energies of the $C_2H_4 + O_3$ and $C_2H_4 + NO_3$ reactions were 6.58 and 6.66 kcal/mol respectively and the Arrhenius expressions of these two reactions were $k = 9.45 \times 10^{11} \exp(-30834/RT)$ and $k = 9.47 \times 10^{12} \exp(-31111/RT)$ ($cm^3 mol^{-1} s^{-1}$), respectively. By comparing, it can be found that the rate constant of the $C_2H_4 + NO_3$ reaction is much larger than that of the $C_2H_4 + O_3$ reaction, which indicated that the NO_3 radical have much stronger ability to degrade ethylene than the O_3 radical.

Furthermore, the theoretical results obtained by employing Quantum chemical calculation in this paper were in good agreement with the experimental results, which indicated that the mechanism and kinetic study by employing quantum chemical calculation in this paper was reasonable and reliable. The theoretical results in this paper will supply important theory basis for establishing kinetic model of the ethylene removal in flue gas by ozone injection. In order to get a more veracious understanding of the VOCs removal in flue gas by ozone injection, more complex alkenes and other VOCs will be selected as objects in the further investigation.

ACKNOWLEDGEMENTS

The authors acknowledged the financial support of the Key Project of the Chinese National Programs for Fundamental Research and Development (2006 CB200303) and the National Science Foundation for Distinguished Young Scholars (50525620).

REFERENCES

1. J.S. Chang, K. Urashima, Y.X. Tong, W.P. Liu, H.Y. Wei, F.M. Yang and X.J. Liu, *J. Electrostat.*, **57**, 313 (2003).
2. M.T. Izquierdo, B. Rubio, C. Mayoral and J.M. Andres, *Fuel*, **82**, 147 (2003).
3. Y.H. Lee, W.S. Jung, Y.R. Choi, J.S. Oh, S.D. Jang, Y.G. Son, M.H. Cho and W. Namkung, *Environ. Sci. Technol.*, **37**, 2563 (2003).
4. J.B. Jarvis, A.T. Day, N.J. Suchak, LoTOx™ Process Flexibility and Multipollutant Control Capability, Combined Power Plant Air Pollutant Control Mega Symposium Washington, DC, pp. 19-22 (2003)
5. Y. Fu and U.M. Diwekar, *Adv. Environ. Res.*, **8**, 173 (2003).
6. Y.S. Mok and H.J. Lee, *Fuel Processing Technol.*, **87**, 591 (2006).
7. L.S. Wei, J.H. Zhou, Z.H. Wang and K.F. Cen, *Ozone: Sci. Eng.*, **29**, 207 (2007).
8. Z.H. Wang, J.H. Zhou, Y.Q. Zhu, Z.C. Wen and K.F. Cen, *Fuel Process. Technol.*, **88**, 817 (2007).
9. J.T. Herron and R.E. Huie, *J. Am. Chem. Soc.*, **99**, 5430 (1977).
10. R.I. Martinez, J.T. Herron and R.E. Huie, *J. Am. Chem. Soc.*, **103**, 3807 (1981).
11. R. Atkinson, *J. Phys. Chem. Ref. Data*, **20**, 459 (1991).
12. M.J. Frisch, G.W. Trucks, J.A. Pople, et.al., Gaussian 03. Gaussian, Inc., Pittsburgh, PA (2003).
13. C. Lee, W. Yang and R.G. Parr, *Phys. Rev. B*, **37**, 785 (1988).
14. A.D. Becke, *J. Chem. Phys.*, **98**, 5648 (1993).
15. C. Gonzalez and H.B. Schlegel, *J. Chem. Phys.*, **90**, 2154 (1989).
16. J. Gauss and C. Cremer, *Chem. Phys. Lett.*, **150**, 280 (1988).
17. E.A. Salter, G.W. Trucks and R.J. Bartlett, *J. Chem. Phys.*, **90**, 1752 (1989).
18. J.B. Foresman, A. Frisch, Exploring Chemistry with Electronic Structure Methods, Gaussian, Pittsburgh, PA, edn. 2 (1996).
19. A.P. Scott and L. Random, *J. Phys. Chem.*, **100**, 16502 (1996).
20. M. Olzmann, E. Kraka, D. Cremer, R. Gutbrod and S. Andersson, *J. Phys. Chem.*, **101**, 9421 (1997).
21. J.M. Anglada, R. Crehuet and J.M. Bofill, *Chem. Eur. J.*, **5**, 1809 (1999).
22. I. Ljubic and A. Sabljic, *J. Phys. Chem. A*, **106**, 4745 (2002).
23. M.F. Hendrickx and C. Vinckier, *J. Phys. Chem. A*, **107**, 7574 (2003).
24. R. Atkinson, D.L. Baulch, R.A. Cox, R.F. Hampson Jr., J.A. Kerr, M.J. Rossi and J. Troe, *J. Phys. Chem. Ref. Data*, **26**, 521 (1997).
25. C. Pfrang, M.D. King, C.E. Canosa-Mas and R.P. Wayne, *Atmos. Environ.*, **40**, 1170 (2006).

(Received: 15 December 2009;

Accepted: 12 May 2010)

AJC-8696